Lanthanide Polyoxocationic Complexes: Experimental and Theoretical Stability Studies and Lewis Acid Catalysis

ARTICLE *in* CHEMISTRY · NOVEMBER 2011

Impact Factor: 5.73 · DOI: 10.1002/chem.201101754 · Source: PubMed

DOI: 10.1002/chem.201101754

Lanthanide Polyoxocationic Complexes: Experimental and Theoretical Stability Studies and Lewis Acid Catalysis

Hani El Moll,[a] Brigitte Nohra,[a] Pierre Mialane,[a] Jérôme Marrot,[a] Nathalie Dupré,[b] Benoît Riflade,[b] Max Malacria,[b] Serge Thorimbert,[b] Bernold Hasenknopf,[b] Emmanuel Lacôte,*[b, d] Pablo A. Aparicio,[c] Xavier López,[c] Josep M. Poblet,*[c] and Anne Dolbecq*[a]

Abstract: The [ε-$PMo^{V}_{8}Mo^{VI}_{4}O_{36}(OH)_4\{Ln^{III}(H_2O)\}_4]^{5+}$ (Ln = La, Ce, Nd, Sm) polyoxocations, called **εLn$_4$**, have been synthesized at room temperature as chloride salts soluble in water, MeOH, EtOH, and DMF. Rare-earth metals can be exchanged, and ^{31}P NMR spectroscopic studies have allowed a comparison of the affinity of the reduced {ε-PMo_{12}} core, thus showing that the La^{III} ions have the highest affinity and that rare earths heavier than Eu^{III} do not react with the ε-Keggin polyoxometalate. DFT calculations provide a deeper insight into the geometries of the systems studied, thereby giving more accurate information on those compounds that suffer from disorder in crystalline form. It has also been confirmed by the hypothetical La→Gd substitution reaction energy that Ln ions beyond Eu cannot compete with La in coordinating the surface of the ε-Keggin molybdate. Two of these clusters (Ln = La, Ce) have been tested to evidence that such systems are representative of a new efficient Lewis acid catalyst family. This is the first time that the catalytic activity of polyoxocations has been evaluated.

Keywords: catalysis · density functional calculations · lanthanides · molybdenum · polyoxometalates

Introduction

Polyoxometalates (POMs) are a class of soluble metal oxide clusters with a large variety of structures and properties that are attracting an ever-growing interest.[1] Among these properties, catalysis is of primary importance.[2] Whereas Brønsted acid and redox catalytic activity[3] has been studied for several decades, Lewis acid catalysis has only recently been evidenced for POMs.[4] Indeed, it has been shown that the introduction of Lewis acidic cations onto polyoxotungstate frameworks can lead to recoverable catalysts that can exhibit high chemoselectivities. In terms of lanthanide-containing POM compounds, the scope of POMs for which catalytic efficiencies have been evidenced remains quite limited. Indeed, only Keggin or Dawson-type monosubstituted polyoxotungstates have been considered so far. The catalytic ability of these compounds has been shown to be strongly dependent on their structural type (Keggin versus Dawson) and chemical composition (nature of the rare-earth metal inserted). The development of this field then requires the investigation of various systems for which the chemical composition (for example, the use of polyoxomolybdates versus polyoxotungstates) and/or the number of Lewis acidic cations grafted on the POM matrix would be modulated.

A few years ago, some of us showed that it is possible to isolate a POM in which four lanthanum cations cap an {ε-$PMo_{12}O_{40}$} framework, an isomer of the {α-$PMo_{12}O_{40}$} Keggin structure that results from successive 60° rotations around the three-fold axes of the M_3O_{13} constituting units (Figure SI1 in the Supporting Information).[5] Halide salts of this eight-electron-reduced POM [ε-$PMo^{V}_{8}Mo^{VI}_{4}O_{36}(OH)_4\{La(H_2O)_4\}_4]^{5+}$ (**εLa$_4$**) have thus been structurally characterized. It should be noted that similar structural types have also been encountered with 3d or 4d capping cations, such as Mo^{VI},[6] Ni^{II},[7] Co^{II},[8] or Zn^{II}[9,10] ions, whereas the {ε-$PMoO_{12}$} isomer has never been ob-

[a] Dr. H. E. Moll, Dr. B. Nohra, Prof. P. Mialane, Dr. J. Marrot, Dr. A. Dolbecq
Institut Lavoisier de Versailles, UMR 8180
Université de Versailles Saint-Quentin en Yvelines
45 Avenue des Etats-Unis
78035 Versailles CEDEX (France)
E-mail: dolbecq@chimie.uvsq.fr

[b] Dr. N. Dupré, B. Riflade, Prof. M. Malacria, Prof. S. Thorimbert, Prof. B. Hasenknopf, Dr. E. Lacôte
UPMC Univ. Paris 6
Institut Parisien de Chimie Moléculaire, CNRS
UMR 7201, 4 Place Jussieu, C. 229, 75005 Paris (France)
E-mail: emmanuel.lacote@icsn.cnrs-gif.fr

[c] P. A. Aparicio, X. López, J. M. Poblet
Departament de Química Física i Inorgànica
Universitat Rovira i Virgili, Marcel.li Domingo s/n
43007 Tarragona (Spain)
E-mail: josepmaria.poblet@urv.cat

[d] Dr. E. Lacôte
Institut de Chimie des
Substances Naturelles CNRS, Avenue de la Terrasse
91198 Gif-sur-Yvette CEDEX (France)

Supporting information for this article is available on the WWW under http://dx.doi.org/10.1002/chem.201101754.

served "naked," probably because of its high negative charge. There has only been one report on catalytic studies on derivatives of the {ε-$PMo_{12}O_{40}$} POMs. Since the neutral 3d-capped POMs are insoluble in common solvents, they have been tested as heterogeneous catalysts for the aerobic oxidation of aldehydes.[11] **εLa$_4$** represents a unique candidate for catalytic Lewis acid studies, as this compound 1) contains four exposed rare-earth centers compared to the previously considered systems with only one 4f embedded center, 2) offers the opportunity to investigate the activity of polyoxomolybdates, whereas to date only polyoxotungstates have been studied, and 3) represents a rare example of positively charged molecular oxide in contrast with all the negatively charged compounds considered so far. **εLa$_4$** thus offers a unique opportunity to enlarge the scope of Lewis acidic POM chemistry, considering also that the nature of the lanthanide cation that constitutes such a Keggin POM can be modulated. We thus describe herein the synthesis of three new **εLn$_4$** species (Ln = Ce, Nd, Sm). Their structures and their behavior in aqueous solution have been thoroughly studied. Density functional theory (DFT) calculations have been performed to accurately pinpoint the location of the Mo^V and Mo^{VI} centers, and to understand the lability of the halide ions, the stability of {ε-PMo_{12}} versus {ε-PW_{12}} cores, and the influence of the nature of the rare earth on the stability of the {ε-PMo_{12}} unit. Two polyoxocations (**εLa$_4$**, **εCe$_4$**) have been tested for the first time as Lewis acids for Mannich-type reactions, thereby evidencing that such systems represent a new efficient Lewis acid catalyst family.

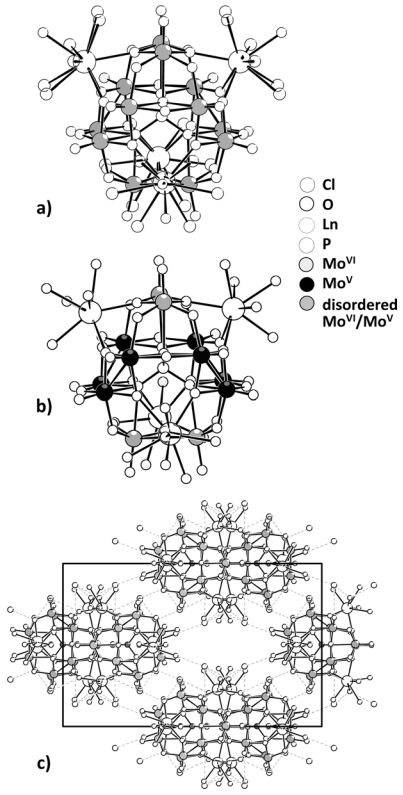

Figure 1. Ball-and-stick representation of a) **εCe$_4$**Cl_5, 1.25 chloride ions are disordered over six positions on each Ce ion, and the 8 Mo^V and 4 Mo^{VI} ions are disordered over twelve positions; b) **εSm$_4$**, the Mo^{VI} and Mo^V ions are localized; c) view of the unit cell of **εSm$_4$**Cl_5 showing the positions of the chloride counterions.

Results and Discussion

Structures: The chloride salts of **εCe$_4$** and **εLa$_4$** are isostructural and crystallize in the $P\bar{4}3m$ space group, whereas the chloride salt of **εSm$_4$** crystallizes in the $I4_122$ space group, a space group with a lower symmetry, which thus allows one to determine more structural information. The overall structure of the {ε-$PMo_{12}O_{40}$} Keggin core in **εSm$_4$** is identical to that of **εLa$_4$**: twelve Mo ions in distorted octahedral coordination surround a central tetrahedral P ion (Figure 1). Valence bond calculations (Figure SI2 in the Supporting Information) together with an examination of the Mo···Mo distances have confirmed the presence of eight Mo^V and four Mo^{VI} ions on **εSm$_4$** and have also shown that four bridging oxygen atoms are protonated. Indeed, Mo^V ions form diamagnetic pairs with Mo^V···Mo^V distances of around 2.6 Å compared to longer Mo^{VI}···Mo^{VI} distances of around 3.2 Å. The protons are located on oxygen atoms that bridge two Mo^V ions. This determination has not been possible on **εCe$_4$** because of the disorder induced by the cubic symmetry (Figure SI3 in the Supporting Information). In both structures, besides four protons, four capping lanthanide cations compensate the high negative charge of the eight-electron-reduced $[PMo^V_8Mo^{VI}_4O_{40}]^{11-}$ Keggin core. These Ln ions (Ln = Ce, Sm) are bound to the POM core through Ln–O bounds with three bridging oxygen atoms (Figure 1a and b). The counterions of the $[PMo^V_8Mo^{VI}_4O_{36}(OH)_4Ln_4]^{5+}$ polycationic species are Cl^- anions. However, differences can be highlighted; in **εCe$_4$**, the five chloride ions are disordered and have been located with partial occupancy factors on a position close to the Ce ions at a distance equal to 2.73(4) Å (Figure 1a), slightly longer than the Ce–O distance of approximately 2.5 Å usually observed for water molecules bound to the rare-earth cation. A similar situation had been encountered for **εLa$_4$**, whereas in **εSm$_4$** the chloride ions are not bound to the Sm ions, all the positions close to these Sm ions being at distances shorter than 2.52 Å. Only two of the five chloride ions have been located. They occupy vacant spaces between the cationic POMs (Figure 1c) with Cl···O distances between the anions and the oxygen of the **εSm$_4$** cations around 3.2 Å. In both structures, the coordination sphere of the Ln ions is completed by water molecules. It has not been possible to obtain crystals of **εNd$_4$**Cl_5 of sufficient quality for single-crystal X-ray diffraction. However, a comparison of the powder X-ray diffraction patterns (Figure SI4 in the Supporting Information) has allowed us to determine that **εNd$_4$**Cl_5 crystallizes in the same space group as **εSm$_4$**Cl_5.

Synthesis and ^{31}P NMR spectroscopic studies of lanthanide exchange: The synthesis of the chloride salts of the **εLn$_4$**

(Ln = Ce, Nd, Sm) polyoxoions was performed by the reaction of a solution of Mo^{V} ions, to which are added Mo^{VI} ions, HPO_4^{2-}, and $LnCl_3$, following the experimental procedure described for **εLa$_4$**.[5] Dark red cubic crystals were obtained by slow evaporation of the solution in moderate (**εCe$_4$**) to poor (**εNd$_4$** and **εSm$_4$**) yield. It was not possible to isolate similar compounds with rare earths heavier than Sm. Furthermore, the use of a nitrate salt of the lanthanide precursor does not allow isolation of the **εLn$_4$** POMs, thereby showing that the presence of chloride ions is essential for their formation. The purity of the phases has been checked by comparison of the experimental X-ray powder pattern with the powder pattern calculated from the structure solved from single-crystal X-ray diffraction data (Figure SI4 in the Supporting Information). The **εLn$_4$** POMs are soluble in water, MeOH, DMF, EtOH, only slightly soluble in CH_3CN, and give red solutions. The ^{31}P NMR spectrum of **εCe$_4$**Cl_5 dissolved in water reveals three resonances at $\delta =$ 21.47, 36.10, and 36.42 ppm and with relative intensities of 1:0.25:0.46 (Figure 2a). The resonances at $\delta = 36.10$ and

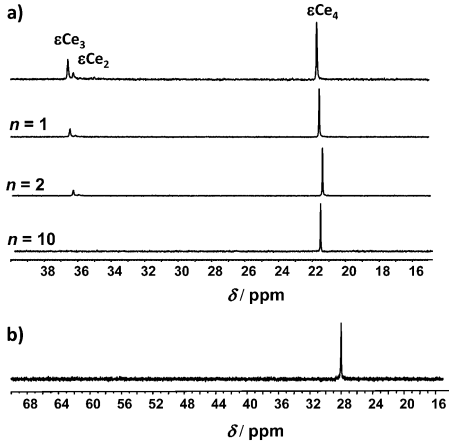

Figure 2. ^{31}P NMR spectra of a) **εCe$_4$** dissolved in water at room temperature and after addition of an increasing amount of $CeCl_3$ with the attribution of the peaks (see text) and b) **εCe$_4$** dissolved in MeOH; n is defined as the ratio between the concentration of $CeCl_3$ added and the polyoxocationic species.

36.42 ppm progressively disappear by addition of increasing quantities of $CeCl_3$. A similar behavior had been observed for **εLa$_4$**Cl_5, but for which only two peaks were initially observed, and had been interpreted by the existence of an equilibrium between the species with four capping La ions and the species with only three capping La ions. Considering similar behavior, two equilibria can be postulated in the case of **εCe$_4$**, the first one between the polycation with four Ce and the polycation with three Ce (denoted **εCe$_3$**) and the second one between **εCe$_3$** and the species with only two Ce ions (denoted **εCe$_2$**) [Eqs. (1) and (2)]:

$$\varepsilon\mathbf{Ce_4} \rightleftharpoons \varepsilon\mathbf{Ce_3} + Ce^{III} \quad (1)$$

$$\varepsilon\mathbf{Ce_3} \rightleftharpoons \varepsilon\mathbf{Ce_2} + Ce^{III} \quad (2)$$

The attribution of the peaks is shown in Figure 2a. The ^{31}P NMR spectrum of **εCe$_4$** dissolved in MeOH is strikingly different as it only exhibits one resonance at $\delta = 28.01$ ppm (Figure 2b), thus showing that decomplexation of the capping rare earth is far less favorable in this nonaqueous solvent. Note, however, that it has not been possible to record the ^{31}P NMR spectrum of **εCe$_4$** dissolved in CH_3CN, the solvent used in catalytic studies (see below) due to its poor solubility.

We have then studied the rare-earth exchange on the **εLn$_4$** polyoxoions, starting with **εLa$_4$**. When $CeCl_3$ is added to a solution of **εLa$_4$**, four new peaks progressively appear (Figure 3). These peaks are attributed to species in which 1

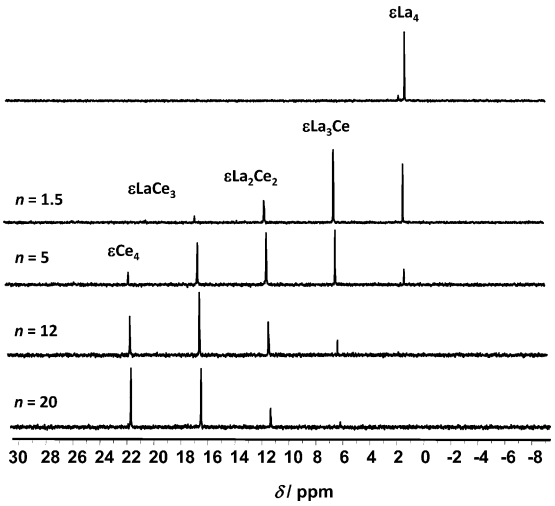

Figure 3. ^{31}P NMR spectra of **εLa$_4$** dissolved in water at room temperature and after addition of an increasing amount of $CeCl_3$ with the attribution of the peaks (see text); n is defined as the ratio between the concentration of $CeCl_3$ added and of the polyoxocationic species.

to 4 La ions have been exchanged by Ce ions, thus forming **εLa$_3$Ce**, **εLa$_2$Ce$_2$**, **εLaCe$_3$**, and **εCe$_4$** species, respectively [Eqs. (3), (4), (5), and (6)]:

$$\varepsilon\mathbf{La_4} + Ce^{III} \rightleftharpoons \varepsilon\mathbf{La_3Ce} + La^{III} \quad (3)$$

$$\varepsilon\mathbf{La_3Ce} + Ce^{III} \rightleftharpoons \varepsilon\mathbf{La_2Ce_2} + La^{III} \quad (4)$$

$$\varepsilon\mathbf{La_2Ce_2} + Ce^{III} \rightleftharpoons \varepsilon\mathbf{LaCe_3} + La^{III} \quad (5)$$

$$\varepsilon\mathbf{LaCe_3} + Ce^{III} \rightleftharpoons \varepsilon\mathbf{Ce_4} + La^{III} \quad (6)$$

The evolution of the proportions of the various substituted species is shown in Figure SI5 in the Supporting Information. The **εLa$_4$** POM initially present has totally disappeared after the addition of 7 equiv of $CeCl_3$; **εLa$_3$Ce** is a transitory species that forms and then disappears after addition of 16 equiv of $CeCl_3$, whereas the **εLa$_2$Ce$_2$** and **εLaCe$_3$** species never disappear even after addition of a large excess

amount of $CeCl_3$ (up to 40 equiv). A symmetrical experiment has been performed with **εCe$_4$** as the starting reactant to which increasing amounts of $LaCl_3$ were added (Figure SI6 in the Supporting Information). Only two peaks remained after the addition of 40 equiv of $LaCl_3$, which are attributed to **εLa$_3$Ce** and **εLa$_4$**. The comparison of these two experiments indicates that the **εLa$_4$** POM is more stable than the **εCe$_4$** POM. To compare quantitatively the stability of the **εLn$_4$** POMs, 4 equiv of $LnCl_3$ (Ln = Ce, Nd, Sm, Eu) have been added to a solution of **εLa$_4$**, thus leading to a mixture of **εLa$_4$**, **εLa$_3$Ln**, **εLa$_2$Ln$_2$**, **εLaLn$_3$**, and **εLn$_4$** complexes. The proportion of each species has been deduced from the integration of the peaks. The following relative stability constant can be written as Equation (7):

$$K_{rel} = [La]_{complex}/[Ln]_{complex} \quad (7)$$

in which $[Ln]_{complex}$ is the concentration of the complexed rare earth in all its forms. This constant allows a comparison between the affinity of the La and of various Ln cations for the {ε-PMo_{12}} core. If we make the hypothesis that the four sites on the POM core are equivalent and independent, and considering a binomial law, it then follows that [Eq. (8)]:

$$K_{rel} = (4[\varepsilon\mathbf{La_4}] + 3[\varepsilon\mathbf{La_3Ln}] + 2[\varepsilon\mathbf{La_2Ln_2}] + [\varepsilon\mathbf{LaLn_3}])/ ([\varepsilon\mathbf{La_3Ln}] + 2[\varepsilon\mathbf{La_2Ln_2}] + 3[\varepsilon\mathbf{LaLn_3}] + 4[\varepsilon\mathbf{Ln_4}]) \quad (8)$$

The values of K_{rel} for various rare-earth metals as a function of their ionic radii[12] are reported in Figure 4. These experiments show that La^{III} is the rare-earth cation that has the highest affinity for the ε-Keggin core, and there is no exchange for rare-earth cations with ionic radii smaller than Eu^{III}.

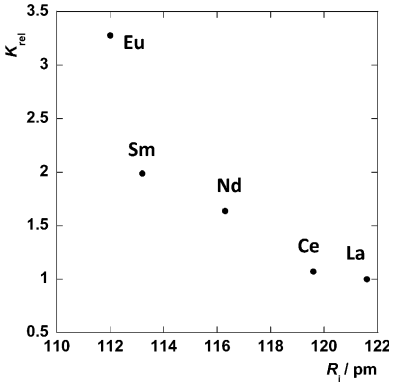

Figure 4. Value of the relative constant K_{rel} representing the ratio between the affinity of the La and that of various Ln^{III} (Ln = Ce, Nd, Sm, Eu) rare-earth cations for the {ε-PMo_{12}} core as a function of the ionic radii of the Ln^{III} cations.

DFT calculations: DFT studies driven on polyoxometalates have largely proven to give valuable information about structure, relative stability, electronic properties, and so on.[13–15] In the present work, we deal with rather intricate structures from the geometrical point of view due to the presence of a large number of labile ligands (H_2O, Cl^-). In this section, we aim to provide additional information about the geometry of **εLa$_4$**, such as the positions of the chloride atoms, disordered by X-ray characterization. Also, we wish to rationalize the correct distribution of the eight metal electrons over the {ε-PMo_{12}} framework. By working with a model compound that contains Gd, we will get a qualitatively correct experimental trend of stabilities from the calculations driven on two lanthanide-PMo_{12} compounds.

Rotational isomers of $PMo_{12}O_{40}$: Among the five rotational isomers of the $XMo_{12}O_{40}$ Keggin anion (e.g., α, β, γ, δ, and ε) proposed by Baker and Figgis,[16] the ε form, obtained by 60° rotation of the four Mo_3O_{13} triads, presents unique electronic and geometric features. In particular, {ε-PMo_{12}} is unknown in the fully oxidized form. DFT calculations confirm that this isomer is very unstable (+45.6 kcal mol^{-1} with respect to α) due to the presence of six pairwise short Mo^{VI}–Mo^{VI} contacts[17] computed to be d_{Mo-Mo} = 2.99 Å. These destabilizing interactions appear after the second Mo_3 rotation. The most common isomers, α and β, do not present any of these Mo–Mo close contacts, so they are the most stable forms of the series. The γ form presents one of such close contacts, and its energy is +10.4 kcal mol^{-1} higher than the α isomer. The δ isomer with three Mo–Mo contacts has an E_{rel} = +25.2 kcal mol^{-1} (see Table 1 for the full data). Thus, each Mo–Mo close contact present in the oxidized structure causes a destabilization of approximately 8–10 kcal mol^{-1} considering the idealized maximal symmetry of the compounds. It is well known that polyoxomolybdates may present a significant Pfeiffer effect.[18,19] Their chirality results from a structural distortion recently analyzed by theoretical methods and attributed to a second-order Jahn–Teller effect.[20] However, $[PMo_{12}O_{40}]^{3-}$ is poorly distorted and its energy very close to the undistorted one. The homologous tungstates behave similarly within the α–ε series,[21] although featuring a somewhat larger destabilization per W–W contact (Table 1). Previously reported DFT calculations on Keggin isomers showed the determinant role of bonding Mo orbitals in the stabilization of the epsilon form.[22] Let us

Table 1. Binding energies of oxidized and 8-electron-reduced (in parentheses) anions computed relative to the α forms, and HOMO–LUMO gaps for the five Baker–Figgis isomers of the Keggin anion.

Isomer (no. rotated triads)	M–M close contacts	$[PMo_{12}O_{40}]^{3-}$ E_{rel} [kcal mol^{-1}]	E(LUMO) [eV]	$[PW_{12}O_{40}]^{3-}$ E_{rel} [kcal mol^{-1}]
α	0	0.0 (0.0)	−4.98	0.0 (0.0)
β (1)	0	+5.4	−5.12	+4.6
γ (2)	1	+10.4	−5.09	+13.9
δ (3)	3	+25.2	−5.03	+30.7
ε (4)	6	+45.6 (−5.0)	−4.89	+55.9 (+11.2)
		This work		Ref. [21]

take the optimized structures of the oxidized {α-PMo_{12}} and {ε-PMo_{12}} anions and their sequence of molecular orbitals (MOs). Even if the lowest unoccupied MO is found at a similar energy in the α and ε isomers (−4.98 eV versus −4.89 eV, respectively), their nature varies from isomer to isomer. In the α isomer they are formally nonbonding combinations of d_{xy} molybdenum orbitals, and reduction of this compound produces no appreciable structural changes. On the other hand, the first six empty MOs in the ε isomer have Mo–Mo bonding character that leads to notable geometrical changes upon reduction. Our results show that Mo–Mo close contacts shorten from 2.99 Å in the fully oxidized form to 2.83 Å in the 8-electron-reduced naked $[\varepsilon\text{-}PMo_{12}O_{40}]^{11-}$ anion. At this stage, the ε isomer becomes more stable than the α isomer by about 5.0 kcal mol^{-1}. Such highly reduced molecules are unstable in the naked form due to the high negative charge that must be compensated by counterions attached to the POM surface, such as the $[ML_n]^{q+}$ cationic units to the ε isomer. We want to stress that the eight-fold-reduced {ε-PW_{12}} is still higher in energy (+11.2 kcal mol^{-1}) than its eight-electron α counterpart. The situation with localized electrons in W–W bonding MOs is less advantageous than in molybdates, as shown by Rohmer et al. for the 2-electron-reduced {γ-SiW_{12}}.[23] In this molecule, with one W–W short contact, electrons delocalize over the available d_{xy} W orbitals of nonbonding character rather than in the bonding W–W molecular orbital. These are pieces of evidence that might explain why ε-Keggin tungstates are unknown.

Structural characterization of ***εLa₄*** *and* ***εLa₃Gd***: Finding energy minima for the structures discussed in the present paper is a difficult task at a standard computational level. The origin is the flat potential-energy surfaces associated to them. The large number of external aqua groups that stabilize the capping Ln^{III} ions and their high mobility are responsible for the shape of the potential-energy surface. Geometry optimizations were carried out with the standard tight convergence thresholds, thereby allowing the optimization algorithm to explore a large part of the potential-energy surface until a flat region of low energy (although not a real minimum) is reached. For the purpose of the present computational study, the structures obtained were of sufficient quality (see also numerical values in Table 2). From our point of view, this strategy gives better results and more stable structures than just lowering the thresholds to looser values to assure convergence.

Table 2. Selected averaged DFT versus X-ray geometrical parameters for **εLa₄**Cl_5 [Å]. The DFT parameters for the monocationic species **εLa**Cl_4^+ are included for comparison.

	DFT		X-ray
	εLa₄Cl_4^+	**εLa₄**Cl_5	**εLa₄**Cl_5
Mo^{VI}–Mo^{VI} (2×)	3.191	3.183	3.10[24]
Mo^{V}–Mo^{V} (4×)	2.618	2.618	2.60[24]
La–Cl	2.848	2.823	2.795
La–O_{POM} (short)	2.514	2.479	disordered
La–O_{POM} (long)	2.652	2.613	
La–O_{POM} (avg)	2.518	2.524	2.55
La–O_w (equatorial)	2.594	2.611	2.591
La–O_w (apical)	2.591	2.606	2.745

In the X-ray characterization of the **εLa₄**Cl_5 system, one of the five Cl atoms could not be fully determined, thereby suggesting that it is not fully linked to any La ion. Thus, a molecule with four chloride atoms must be almost equal in what concerns the main geometrical parameters, so the first system tackled by DFT is $[\varepsilon\text{-}PMo_{12}O_{36}(OH)_4\{La(H_2O)_4Cl\}_4]^+$, **εLa₄**$Cl_4^+$, a monocationic model compound with four chloride atoms of the experimentally observed neutral compound. For the optimization of this system, the initial positions of aqua and Cl ligands were deduced from the X-ray data, though there is some disorder. A 130-cycle geometry optimization run with standard convergence parameters led the molecule to a flat region in the potential surface with energy oscillations smaller than 1 kcal mol^{-1}. This is a tiny value over the total energy of the molecule and we consider any of the structures included in this energy range as a stable form of the compound. The analysis of the geometry allows us to confirm that the structure makes sense and greatly resembles that of **εLa₄**. We want to stress that present calculations fully reproduce the typical electron distribution of eight metal electrons expected in the {ε-PMo_{12}} Keggin cluster. In fact, the **εLa₄** structure presents disorder due to the cubic symmetry, and the Mo–Mo distances cannot be resolved precisely. DFT results allow us to distinguish the eight Mo^V ions from the four Mo^{VI} ions, and all the Mo–Mo distances are in accordance with what is expected for four short and two long Mo–Mo distances. Short ones (2.618 Å) correspond to two bonded Mo^V atoms, whereas long ones (3.191 Å) are characteristic of nonbonded Mo^{VI} atoms. Previously reported X-ray short and long Mo–Mo distances for the reduced {ε-PMo_{12}} compound are 2.60 and 3.10 Å, respectively.[24] A list of relevant computed interatomic distances is shown in Table 2. The composition and occupation of the molecular orbitals for this structure explain such geometrical parameters. The four highest occupied orbitals are of Mo–Mo bonding nature, whereas the two lowest unoccupied are of the same nature but with a poorer overlap due to the longer Mo–Mo distance (Figure 5). From population analysis (multipole derived charges) it arises that eight Mo centers carry a positive charge notably smaller than the other four (2.0 over 2.6), in accordance to the molecular orbital occupations.

Present DFT calculations allow us to give more geometrical information than the quite disordered X-ray data. The computed La–O_{POM} distances can be classified into short (2.514 Å) and long (2.652 Å), though the average of them is 2.518 Å, very close to the experimental 2.55 Å. The monocationic **εLa₄**Cl_4^+ structure contains several hydrogen bonds between water hydrogen atoms and bridging oxygen atoms of the POM framework, which stabilize the water ligands within the structure.

For the neutral compound, **εLa₄**Cl_5, we carried out equivalent calculations. The starting geometry corresponds to the final one obtained for **εLa₄**Cl_4^+ by DFT optimization with

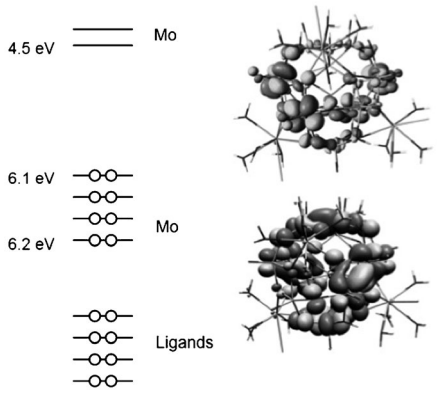

Figure 5. Molecular orbital diagram obtained from DFT calculations, with the four doubly occupied Mo–Mo bonding orbitals, and the two empty Mo–Mo orbitals, along with a 3D representation of one of each.

an additional chloride atom. Since there is no clear experimental clue of the position of the fifth chloride atom, we put it at bonding distance from one of the four La^{III} ions, with a plausible distribution of the other ligands linked to the same La. After 200 optimization cycles without reaching full convergence but having achieved a flat potential-energy region, one of the five Cl^- ions of the structure was found far from its initial position, just close to three water molecules and stabilized by hydrogen bonds. This confirms the X-ray observations in the sense that one chloride position cannot be resolved. It actually remains in the surroundings of the POM structure without being strongly bound to it and in principle rather mobile, whereas the other four Cl atoms remain linked to La ions. Table 2 summarizes DFT-computed and X-ray interatomic distances for the neutral compound. The other important features of the system, such as the Mo–Mo distances, are also satisfactorily reproduced in this calculation. DFT calculations have completely determined the existence of eight bonding (localized) metal electrons. The protons bound to μ-O sites of the structure (–OH groups) and the positions of chlorides obtained are in very good agreement with previous experimental characterizations performed by some of us.[5]

Now we analyze some structural features of another lanthanide derivative of the {ε-PMo_{12}} ion. The experimental data collected for compounds with Ln = La, Ce, Nd, Sm, and Eu show that the stability of the Ln-tetracapped ε-Keggin systems diminishes from left to right in the period, a fact tentatively attributed to the size of Ln^{3+}. To know more about this, we studied the replacement of La^{3+} by Gd^{3+} and checked the geometrical features. Justification of this model structure is based on the electronic configuration of Ln^{3+} cations. Gd^{3+} has a half-filled f valence shell (f^7), which is much easier to handle computationally than cations with otherwise-filled valence shells such as f^{1-6} (Sm is a f^5). In addition, Gd^{3+} can be considered similar enough to Sm^{3+} for a test on the relative stability versus La^{3+}. Therefore our model structure contains three La atoms and one Gd (**εLa$_3$Gd**), and its experimental counterpart is the **εSm$_4$** compound. Substitution of four La by four Gd is much too involved from the technical point of view since four Gd atoms would carry 28 unpaired electrons. With that in mind, we believed that one cation substitution suffices to study the geometrical parameters by La→Gd replacement. Another characteristic of our model compound is that it contains three chloride ligands (one per La atom), which confers a total charge of 2+. However, the COSMO not only mimics the solvent effects but also distributes the negative charge necessary to counterbalance the excess positive charge carried by the POM in this case.

It is interesting not only to describe the final geometry obtained upon optimization but also the starting point. Our first geometry for the **εLa$_3$Gd** derivative contained one Gd ion coordinated by six ligands: $(H_2O)_5+Cl^-$, although we expected it to be coordinated by five. The inclusion of the chloride atom in the coordination sphere of Gd allows us to observe if, during the optimization process, Gd gets rid of it or, on the contrary, an aqua ligand is released. The first geometry of this calculation has d(Gd–Cl) = 2.82 Å and d(Gd–O_w) = 2.56/2.61 Å. After a few optimization geometry steps, these turned into d(Gd–Cl) = 3.03 Å and d(Gd–O_w) = 2.47 Å (averaged), thereby confirming that the chloride ion tends to leave the Gd coordination sphere, whereas the five water ligands not only remain bound but strengthen their interaction to Gd. Other geometrical parameters that confirm the quality of the results obtained with the **εLa$_3$Gd** model are shown in Table 3 in comparison with the X-ray analysis for **εSm$_4$**, which in turn is not affected by disorder. The chloride atoms necessary to compensate the positive charge have not been considered since they lie in undetermined positions far from the Ln environment.

Table 3. Selected DFT geometrical parameters related to the Gd region in the model compound **εLa$_3$Gd**, and the X-ray data for the experimental reference, the **εSm$_4$** molecule. Distances are in Å.

	DFT **εLa$_3$Gd**	X-ray **εSm$_4$**
Gd–O_{POM}	2.315	2.374
	2.373	2.391
	2.517	2.508
Gd–O_w (equatorial)	2.453	2.455
Gd–O_w (apical)	2.507	2.522

*Relative stability of **εLa$_4$** and **εLa$_3$Gd***: The model compound **εLa$_3$Gd** allows us to test the relative energy with respect to **εLa$_4$**. We have demonstrated above that Gd satisfactorily plays the role of Sm in what concerns the structure of capped Keggin systems while being much easier to treat at the DFT level. To quantify the relative stability of the two systems, we propose the following reaction [Eq. (9)]:

$$[\varepsilon\text{-}PMo_{12}La_3\{Gd(H_2O)_5\}]^{2+} + [La(H_2O)_9]^{3+} + Cl^- \xrightarrow{\Delta_r E} [\varepsilon\text{-}PMo_{12}La_3\{La(H_2O)_4Cl\}]^{+} + [Gd(H_2O)_9]^{3+} + H_2O \quad (9)$$

Comparison of molecules with different chemical composition can be studied by means of reaction energies that fulfill conservation of matter, and not directly by comparing computed absolute energies of the molecules.

The free Ln^{3+} ions in solution have been coordinated to nine aqua ligands[25] and fully optimized by following the typical coordination numbers of Ln^{III} ions. The chloride anion has been considered without explicit water molecules around (just the solvent effects introduced by the COSMO) since it is a quite soft ion, the coordination sphere of which is too labile to be precisely determined or modeled. The energy of the process, $\Delta_r E$, determines the relative stability of the La–POM and Gd–POM linkages, respectively. Our calculations revealed that $\Delta_r E = -22$ kcal mol^{-1} in favor of the La_4 form, a rather large reaction energy that indicates a strongly disfavored exchange process in the direction La→Gd, thus matching the fact that the La→Eu exchange is not observed experimentally. It must be pointed out that two replacements of La atoms would cost approximately 45 kcal mol^{-1}, and three replacements around 66 kcal mol^{-1}, up to a value around 90 kcal mol^{-1} for the replacement of all four La ions. We also expect that $\Delta_r E$ would be smaller for ions situated to the left of Gd in the periodic table such as Ce, Nd, or Sm.

Lewis acidic catalysis: Embedding Lewis acidic cations into polyoxometalate structures is a way to graft Lewis acidity to the clusters. This has been studied by some of us[4a,b,e,26] and others.[4c,d] However, all the POMs examined so far had a negative neat charge. On the contrary, the **εLn$_4$** complexes are polyoxocations. Moreover, these systems have four accessible sites for Lewis base complexation. It thus appeared important for us to look at how these features would affect or not the activity. We have used the Mannich reaction as a benchmark of their reactivity.

We selected **εLa$_4$** and **εCe$_4$** as potential catalysts because these compounds are synthesized with a better yield. In a typical experiment, diphenylimine **1** was treated with a slight excess amount of silylenol ether **2** (1.5 equiv) in the presence of 2 mol% of the **εLa$_4$** complex in acetonitrile at room temperature for 3.5 h (Table 4, entry 1). β-Amino ketone **3** was formed in 97% yield (based on an internal standard), and 91% isolated yield (entry 2). The **εCe$_4$** complex worked equally well (entry 7; 94% of **3**). Activity was maintained with a lower loading for both complexes (1 mol%; entries 6 and 10). The two complexes were precipitated in diethyl ether at the end of the reaction, centrifuged, and resubmitted to the reaction conditions. No difference was noticed for the lanthanum derivative in the second run (entry 3), whereas the activity dropped significantly during the third run (entry 4). In contrast, the cerium complex was much less efficient as early as the second run (entry 8). In both cases, however, the reaction reached full completion with time (48 h for La (entry 5); 24 h for Ce (entry 9)).

In all cases, the POMs were not fully soluble. The reaction mixtures were orange, which indicated that some of the

Table 4. Evaluation of the catalysts in a Lewis acidic POM-catalyzed Mannich reaction.

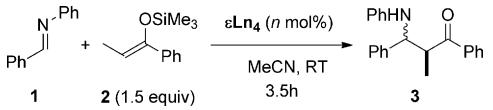

1 2 (1.5 equiv) 3

Entry	Ln	n	Run	Conversion [%]	Yield [%]
1	La	2	1	99	97[a]
2	La	2	1	100	91
3	La	2	2	100	90
4	La	2	3	54[b]	50[a,b]
5	La	2	3	100[c]	90[a,c]
6	La	1	1	96	90
7	Ce	2	1	100	94
8	Ce	2	2	57[b]	51[b]
9	Ce	2	2	100[d]	85[d]
10	Ce	1	1	94	82[a]
11	Ce	<1[e]	1	86[a,c]	82[a,c]
12	Ce	2	1	≈22[a,c,f]	≈15[a,c]

[a] NMR spectroscopic yield (anisole or methyl sulfone internal standard). [b] Conversion and yield were measured after 3.5 h. [c] Reaction took 48 h. [d] Reaction took 24 h. [e] The supernatant from the **εCe$_4$** solution was used as catalyst. [f] Reaction performed in CH_2Cl_2.

εLn$_4$ complexes were solubilized, even if the great majority of the POM remains solid. This raised two issues: 1) What is the nature of the catalysis (heterogeneous or homogeneous), and 2) do the lanthanides dissociate and react as "free" cations? To answer to these two questions, several observations can be reported.

The ^{31}P NMR spectroscopic characterization of **εCe$_4$** seems to indicate that the rare-earth cations are more tightly associated to the polyoxomolybdic backbone in organic solvent than in water (see above). Besides, the absence of blue coloration of the solution during all the catalytic process indicates that no delocalized mixed-valence species are formed by means of oxidation reactions. This suggests that the structure of the POM stayed intact during the course of the reaction, as it has been shown that the decomplexation of La ions from the {ε-PMo_{12}} core is followed by oxidation and leads to molybdenum blue species.[5] Moreover, the ^{31}P NMR spectra of the recovered complexes did not show a significant difference before and after the initial reactions, with only some minor peaks appearing upon recycling.

Concerning the nature of the catalysis, the following experiment was performed. The **εLn$_4$** complexes were dissolved in CH_3CN, centrifuged to remove the insoluble solid, and the orange supernatant (1 mL) was diluted twice. This solution was then used for further catalytic experiments. This still resulted in formation of the Mannich adduct (Table 4, entry 11), albeit much more slowly. Conversely, when the reaction was run in dichloromethane (i.e., a solvent in which the POM is barely soluble as attested by the very pale color of the solution), almost no conversion was observed (entry 12). Taken together, these observations suggest that the catalysis is homogeneous, and that no "free" Ln^{3+} is responsible for the catalysis.

Finally, we examined the chemoselectivity of the two complexes (Scheme 1). Interestingly, both were completely

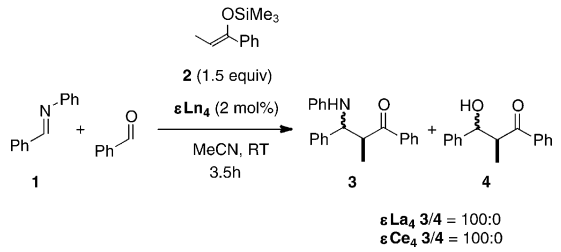

Scheme 1.

chemoselective for diphenylimine over benzaldehyde. In fact, no reaction at all was observed with benzaldehyde.

Overall, mechanistically, both **εLn$_4$** complexes behave quite similarly to the monosubstituted polyoxotungstate $[\alpha_1\text{-}LnP_2W_{17}O_{61}]^{7-}$. Catalysis most likely takes place at the lanthanide centers. As a consequence, the charge has only a minor influence on the reactivity of Ln-substituted polyoxometalates. However, the amount of catalyst needed and the reaction times seem to be largely inferior in the case of **εLn$_4$** species compared to Dawson-type POMs. Furthermore, in the Dawson series, the chemoselectivity (also observed for **εLn$_4$** complexes) was explained by a change in mechanism.[4e] Imines are activated by direct complexation at the lanthanide center, whereas aromatic aldehydes reacted under indirect Brønsted catalysis with a proton generated by complexation of water to the lanthanide. Understanding whether this is a general behavior of POMs that is traceable to the metal oxide framework influence will be an important issue for further study.

Conclusion

In summary, the $[\varepsilon\text{-}PMo^{V}_{8}Mo^{VI}_{4}O_{36}(OH)_4\{Ln(H_2O)_4\}_4]^{5+}$ (Ln = La, Ce, Nd, Sm) polyoxoions, denoted **εLn$_4$**, have been successfully synthesized as chloride salts. ^{31}P NMR spectroscopic studies have allowed us to determine that La^{III} is the rare-earth cation that has the highest affinity for the ε-Keggin core and that the La^{III} ions can only be exchanged by rare-earth cations with ionic radii greater than that of Eu^{III}. Theoretical calculations have been performed to provide a deeper insight into the geometries and reactivity of the systems studied. The natural need for the $\{\varepsilon\text{-}PMo_{12}\}$ isomer to gain electrons originates in the Mo–Mo bonding character of the lowest empty orbitals. Successive reductions of these orbitals compensate the high energy of the fully oxidized ε isomer by 1) reducing the electrostatic repulsions in Mo–Mo contacts, and 2) by filling bonding molecular orbitals. Comparison to tungstate homologues shows that the latter are not likely to be obtained as ε isomers. Calculations carried out on La- and Gd-containing derivatives of the Keggin give complementary information on the structure and the relative stability of such compounds. Firstly, DFT geometries agree very well with X-ray data and provide some extra information in the case of disorder (**εLa$_4$** structure). We have also proven that the La compound is much more stable than the Gd one in solution, a behavior that resembles that of Eu, thereby confirming that the smaller Ln ions are not stable on the surface of the $\{\varepsilon\text{-}PMo_{12}\}$ structure. Catalytic studies have shown that the La and Ce polyoxocations are Lewis acids that catalyze Mannich reactions and are highly chemoselective by favoring activation of imines over aldehydes. Only small quantities of polyoxocation are needed, which corresponds to the saturation concentration of the species in acetonitrile. Future developments will focus on exchanging the chloride counteranions with anionic surfactant to increase the solubility of the compounds in organic solvents.

Experimental Section

Preparation of $[PMo^{V}_{8}Mo^{VI}_{4}O_{36}(OH)_4\{Ce(H_2O)_4\}_4Cl_5]\cdot 11H_2O$ ($\varepsilon Ce_4Cl_5\cdot 11H_2O$): A solution of 0.2 M $\{Mo_2O_4(H_2O)_4\}^{2+}$ was prepared as described.[5] $Na_2MoO_4\cdot 2H_2O$ (0.482 g, 2 mmol), $Na_2HPO_4\cdot 2H_2O$ (0.089 g, 0.5 mmol), and $CeCl_3\cdot 6H_2O$ (19.5 g, 55 mmol) dissolved in water (30 mL) was added to this red solution (20 mL, 4 mmol). The dark blue solution was stirred and the pH was adjusted to 1.8 with 8 M NaOH. Dark red cubic crystals suitable for X-ray diffraction study were collected after one week (0.305 g, 20% based on P). IR: $\tilde{\nu}$ = 1095 (w), 1003 (sh), 991 (sh), 969 (m), 916 (s), 813 (m), 718 (m), 685 (m), 584 cm^{-1} (m); elemental analysis calcd (%) for $H_{58}Ce_4Cl_5Mo_{12}O_{67}P$: H 1.92, Ce 18.37, Cl 5.81, Mo 37.74, P 1.01; found: H 2.06, Ce 18.62, Cl 5.91, Mo 37.75, P 1.04.

Preparation of $[PMo^{V}_{8}Mo^{VI}_{4}O_{36}(OH)_4\{Sm(H_2O)_4\}_4]Cl_5\cdot 28H_2O$ ($\varepsilon Sm_4Cl_5\cdot 28H_2O$): The experimental procedure was identical to **εCe$_4$**; $CeCl_3\cdot 6H_2O$ was replaced by $SmCl_3\cdot 6H_2O$. Dark red cubic crystals suitable for X-ray diffraction study were collected after one week (0.200 g, 11.7% based on P). Elemental analysis indicates that the product is isolated with NaCl and that the formula of the analyzed compound is $[PMo^{V}_{8}Mo^{VI}_{4}O_{36}(OH)_4\{Sm(H_2O)_4\}_4]Cl_5(NaCl)\cdot 28H_2O$. Elemental analysis calcd (%) for $H_{68}Cl_6Mo_{12}NaO_{84}PSm_4$: Cl 6.19, Mo 33.54, Na 0.67, P 0.90, Sm 17.52; found: Cl 6.50, Mo 33.88, Na 0.76, P 0.95, Sm 17.98.

Preparation of $[PMo^{V}_{8}Mo^{VI}_{4}O_{36}(OH)_4\{Nd(H_2O)_4\}_4]Cl_5\cdot 28H_2O$ ($\varepsilon Nd_4Cl_5\cdot 28H_2O$): The experimental procedure was identical to **εCe$_4$**; $CeCl_3\cdot 6H_2O$ was replaced by $NdCl_3\cdot 6H_2O$. Dark red cubic crystals suitable for X-ray diffraction study were collected after one week (0.190 g, 12.4% based on P). Infrared spectra of the **εLn$_4$** species are very close (Figure SI7 in the Supporting Information).

Characterization: Due to the poor yield, no ^{31}P NMR spectroscopic studies were performed for **εNd$_4$** and **εSm$_4$**. Infrared spectra were recorded using an FTIR Magna 550 Nicolet spectrophotometer as pressed KBr pellets. ^{31}P NMR spectra were recorded with ^{1}H decoupling using a Bruker AC-300 spectrometer operating at 121.5 MHz with 5 mm tubes. ^{31}P chemical shifts were referenced to the external standard of 85% H_3PO_4. For all compounds, around 20 mg of sample were dissolved in D_2O (500 μL).

X-ray crystallography: Powder diffraction data was obtained using a Bruker D5000 diffractometer with Cu radiation (1.54059 Å). Single-crystal diffraction data collections were carried out using a Siemens SMART three-circle diffractometer equipped with a CCD bi-dimensional detector using the monochromatized $Mo_{K\alpha}$ wavelength λ = 0.71073 Å. Absorption correction was based on multiple and symmetry-equivalent reflections in the data set using the SADABS program[27] based on the method of Blessing.[28] The structure was solved by direct methods and refined by full-matrix least-squares using the SHELX-TL package.[29]

Crystal data for $\varepsilon Ce_4Cl_5\cdot 11H_2O$: $H_{58}Ce_4Cl_5Mo_{12}O_{67}P$; M_r = 3050.42 g mol^{-1}; cubic; space group $P\bar{4}3m$; a = 12.1559(14) Å; V = 1796.2(4) Å^3; Z = 1; $\mu(Mo_{K\alpha})$ = 4.77 mm^{-1}; 11603 reflections measured, 838 unique; final R_1 = 0.079 and wR_2 = 0.218 ($I > 2\sigma(I)$).

Crystal data for $\varepsilon Sm_4Cl_5{\cdot}28H_2O$: $H_{68}Cl_5Mo_{12}O_{84}PSm_4$; $M_r = 3373.47\ g\,mol^{-1}$; tetragonal; space group $I4_122$; $a = 16.6113(10)$, $c = 26.440(3)$ Å; $V = 7295.7(4)$ Å^3; $Z = 4$; $\mu(Mo_{K\alpha}) = 5.353\ mm^{-1}$; 11603 reflections measured, 838 unique; final $R_1 = 0.058$ and $wR_2 = 0.150$ ($I > 2\sigma(I)$). Further details of the crystal structure investigations can be obtained from the Fachinformationszentrum Karlsruhe, 76344 Eggenstein-Leopoldshafen, Germany (fax: (+49)7247-808-666; e-mail: crysdata@fiz-karlsruhe.de, http://www.fiz-karlsruhe.de/request_for_deposited_data.html) on quoting the depository number CSD-423147 and 423148 for **εCe_4** and **εSm_4**, respectively.

Computational strategy: DFT calculations presented in this work have been obtained using the ADF2009 suite of programs.[30–32] Our calculations are characterized by the generalized gradient approximation (GGA), by applying the Xα model with Becke's corrections[33,34] for describing exchange, and the VWN parameterization[35] with Perdew's corrections[36,37] for correlation (BP86 functional). The electrons were described by Slater-type functions with basis sets of TZP quality for valence electrons. Core electrons were kept frozen and described by single Slater functions (core shells by atom: O 1s; P, Cl 1s–2p; Mo 1s–3d; La, Gd 1s–4d) with core potentials generated using the DIRAC program,[30] and scalar relativistic corrections included by means of the zeroth-order regular approximation (ZORA). All the calculations include the conductor-like screening model (COSMO[38–41]) to account for the solvent effects of water ($\varepsilon = 78.4$). The solvent cavities that surrounded the molecules were created using the solvent-excluding method with fine tesserae. The ionic radii for the atoms that actually define the size of the solvent cavity were chosen to be 0.74 Å for Mo, 1.30 Å for La, 1.19 Å for Gd, 1.20 Å for H, 1.70 for Cl, and 1.52 Å for oxygen. We applied the spin-unrestricted formalism to electronically open-shell species.

Lewis acid catalysis: Diphenylimine (**1**, 0.25 mmol, 45 mg) and the silyl enol ether (**2**, 0.25 mmol; 1 equiv; 51.6 mg) were added to a solution of the catalyst (2 mol%; 16 mg) in CH_3CN (2 mL) at room temperature. The reaction was followed by NMR spectroscopy using anisole or methylsulfone as internal standard. After completion, a solution of acetone/ethanol (1:1) (6 mL) was added, followed by diethylether (60 mL). The catalyst was precipitated, centrifuged, and separated from the reactions products. The remaining organics were concentrated under reduced pressure. The residue was purified by flash column chromatography (petroleum ether/ethyl acetate 90:10) to afford the desired β-amino ketone **3** as a mixture of the two diastereomers.

Acknowledgements

We thank CNRS, UVSQ, UPMC, the French ANR (grant no. 08-PCVI-0005 to E.L., S.T., and B.H.), the Spanish MCINN (CTQ2008-06549-C02-01/BQU), the DURSI of the Generalitat de Catalunya (2009SGR-00462) and the XRTQC for financial support of this work. FR2769 is acknowledged for technical assistance. A.D. thanks Nicolas Queriaux and Dominika Lesnicki for their participation in the synthesis of **εLn_4** species and Sébastien Floquet for fruitful discussions on NMR spectroscopic data. X.L. thanks the Ramón y Cajal program (RYC-2008-02493).

[1] Nonexhaustive list of recent review articles: a) U. Kortz, A. Müller, J. van Slageren, J. Schnack, N. S. Dalal, M. Dressel, *Coord. Chem. Rev.* **2009**, *253*, 2315; b) D.-L. Long, R. Tsunashima, L. Cronin, *Angew. Chem.* **2010**, *122*, 1780; *Angew. Chem. Int. Ed.* **2010**, *49*, 1736; c) B. Keita, L. Nadjo, *J. Mol. Catal. A: Chem.* **2007**, *262*, 190; d) A. Dolbecq, E. Dumas, C. R. Mayer, P. Mialane, *Chem. Rev.* **2010**, *110*, 6009; e) J.-F. Lemonnier, S. Duval, S. Floquet, E. Cadot, *Isr. J. Chem.* **2011**, *51*, 290; f) J. M. Clemente-Juan, E. Coronado, *Coord. Chem. Rev.* **1999**, *193–195*, 361.

[2] a) N. Mizuno, K. Yamaguchi, K. Kamata, *Coord. Chem. Rev.* **2005**, *249*, 1944; b) Polyoxometalates in Catalysis: C. L. Hill, *J. Mol. Catal. A: Chem.* **2007**, *262*, 1–242.

[3] For recent articles, see: a) A. Sartorel, P. Miro, E. Salvadori, S. Romain, M. Carraro, G. Scorrano, M. Di Valentin, A. Llobet, C. Bo, M. Bonchio, *J. Am. Chem. Soc.* **2009**, *131*, 16051; b) A. E. Kuznetsov, Y. V. Geletii, C. L. Hill, K. Morokuma, D. G. Musaev, *Inorg. Chem.* **2009**, *48*, 1871.

[4] a) C. Boglio, G. Lemière, B. Hasenknopf, S. Thorimbert, E. Lacôte, M. Malacria, *Angew. Chem.* **2006**, *118*, 3402; *Angew. Chem. Int. Ed.* **2006**, *45*, 3324; b) C. Boglio, K. Micoine, P. Rémy, B. Hasenknopf, S. Thorimbert, E. Lacôte, M. Malacria, C. Afonso, J.-C. Tabet, *Chem. Eur. J.* **2007**, *13*, 5426; c) Y. Kikukawa, S. Yamaguchi, Y. Nakagawa, K. Uehara, K. Yamaguchi, N. Mizuno, *J. Am. Chem. Soc.* **2008**, *130*, 15872; d) Y. Kikukawa, S. Yamaguchi, K. Tsuchida, Y. Nakagawa, K. Uehara, S. Uchida, K. Yamaguchi, N. Mizuno, *J. Am. Chem. Soc.* **2008**, *130*, 5472; e) N. Dupré, P. Rémy, K. Micoine, C. Boglio, S. Thorimbert, E. Lacôte, B. Hasenknopf, M. Malacria, *Chem. Eur. J.* **2010**, *16*, 7256.

[5] P. Mialane, A. Dolbecq, L. Lisnard, A. Mallard, J. Marrot, F. Sécheresse, *Angew. Chem.* **2002**, *114*, 2504; *Angew. Chem. Int. Ed.* **2002**, *41*, 2398.

[6] a) M. I. Khan, A. Müller, S. Dillinger, H. Bögge, Q. Chen, J. Zubieta, *Angew. Chem.* **1993**, *105*, 1811; *Angew. Chem. Int. Ed. Engl.* **1993**, *32*, 1780; b) M. I. Khan, Q. Chen, J. Salta, C. J. O'Connor, J. Zubieta, *Inorg. Chem.* **1996**, *35*, 1880; c) T. Yamase, E. Ishikawa, *Bull. Chem. Soc. Jpn.* **2008**, *81*, 983.

[7] a) A. Müller, C. Beugholt, P. Kögerler, H. Bögge, S. Bud'ko, M. Luban, *Inorg. Chem.* **2000**, *39*, 5176; b) W. Wang, L. Xu, G. Gao, L. Liu, X. Liu, *CrystEngComm* **2009**, *11*, 2488; c) X.-B. Cui, S.-T. Zheng, G.-Y. Yang, *Z. Anorg. Allg. Chem.* **2005**, *631*, 642.

[8] H.-H. Yu, X.-B. Cui, L. Kong, W.-J. Duan, J.-Q. Xu, T.-G. Wang, *Dalton Trans.* **2008**, 195.

[9] C. Lei, J.-G. Mao, Y.-Q. Sun, J.-L. Song, *Inorg. Chem.* **2004**, *43*, 1964.

[10] a) L. M. Rodriguez Albelo, A. R. Ruiz-Salvador, A. Sampieri, D. W. Lewis, A. Gómez, B. Nohra, P. Mialane, J. Marrot, F. Sécheresse, C. Mellot-Draznieks, R. Ngo Biboum, B. Keita, L. Nadjo, A. Dolbecq, *J. Am. Chem. Soc.* **2009**, *131*, 16078; b) L. M. Rodriguez Albelo, A. R. Ruiz-Salvador, D. W. Lewis, A. Gómez, P. Mialane, J. Marrot, A. Dolbecq, A. Sampieri, C. Mellot-Draznieks, *Phys. Chem. Chem. Phys.* **2010**, *12*, 8632.

[11] D. Sloboda-Rozner, K. Neimann, R. Neumann, *J. Mol. Catal. A: Chem.* **2007**, *262*, 109.

[12] R. D. Shannon, *Acta Crystallogr. Sect. A* **1976**, *32*, 751.

[13] J. M. Poblet, X. López, C. Bo, *Chem. Soc. Rev.* **2003**, *32*, 297.

[14] J. A. Fernández, X. López, C. Bo, C. De Graaf, E. J. Baerends, J. M. Poblet, *J. Am. Chem. Soc.* **2007**, *129*, 12244.

[15] X. López, P. Miró, J. J. Carbó, A. Rodríguez-Fortea, C. Bo, J. M. Poblet, *Theor. Chem. Acc.* **2011**, *128*, 393.

[16] L. C. W. Baker, J. S. Figgis, *J. Am. Chem. Soc.* **1970**, *92*, 3794.

[17] D. L. Kepert, *Inorg. Chem.* **1969**, *8*, 1556.

[18] M. T. Pope, *Inorg. Chem.* **1976**, *15*, 2008.

[19] J. F. Garvey, M. T. Pope, *Inorg. Chem.* **1978**, *17*, 1115.

[20] a) L. Yan, X. López, J. J. Carbó, R. T. Sniatynsky, D. D. Duncan, J. M. Poblet, *J. Am. Chem. Soc.* **2008**, *130*, 8223; b) B. Hasenknopf, K. Micoine, E. Lacôte, S. Thorimbert, M. Malacria, R. Thouvenot, *Eur. J. Inorg. Chem.* **2008**, 5001.

[21] X. López, J. M. Poblet, *Inorg. Chem.* **2004**, *43*, 6863.

[22] F.-Q. Zhang, X.-M. Zhang, H.-S. Wu, Y.-W. Li, H. Jiao, *J. Phys. Chem. A* **2007**, *111*, 1683.

[23] a) M.-M. Rohmer, M. Bénard, E. Cadot, F. Sécheresse in *Polyoxometalate Chemistry: From Topology via Self-Assembly to Applications* (Eds.: M. T. Pope, A. Müller), Kluwer Academic, Dordrecht, The Netherlands, **2001**, pp. 117–133; b) M.-M. Rohmer, M. Bénard, *Chem. Soc. Rev.* **2001**, *30*, 340.

[24] A. Dolbecq, P. Mialane, L. Lisnard, J. Marrot, F. Sécheresse, *Chem. Eur. J.* **2003**, *9*, 2914.

[25] C. Beuchat, D. Hagberg, R. Spezia, L. Gagliardi, *J. Phys. Chem. B* **2010**, *114*, 15590 and references therein.

[26] a) E. Derat, E. Lacôte, B. Hasenknopf, S. Thorimbert, M. Malacria, *J. Phys. Chem. A* **2008**, *112*, 13002; b) M. Bosco, S. Rat, N. Dupré,

B. Hasenknopf, E. Lacôte, M. Malacria, P. Rémy, J. Kovensky, S. Thorimbert, A. Wadouachi, *ChemSusChem* **2010**, *3*, 1249.
[27] G. M. Sheldrick, SADABS; program for scaling and correction of area detector data, University of Göttingen, Germany, **1997**.
[28] R. Blessing, *Acta Crystallogr. Sect. A* **1995**, *51*, 33.
[29] G. M. Sheldrick, SHELX-TL v.5.03, Software Package for the Crystal Structure Determination, Siemens Analytical X-ray Instrument Division: Madison, WI USA, **1994**.
[30] ADF2009.01, SCM, Theoretical Chemistry, Vrije Universiteit, Amsterdam, The Netherlands, http://www.scm.com.
[31] C. Fonseca Guerra, J. G. Snijders, G. Te Velde, E. J. Baerends, *Theor. Chem. Acc.* **1998**, *99*, 391.
[32] G. Te Velde, F. M. Bickelhaupt, S. J. A. van Gisbergen, C. Fonseca Guerra, E. J. Baerends, J. G. Snijders, T. Ziegler, *J. Comput. Chem.* **2001**, *22*, 931.
[33] A. D. Becke, *J. Chem. Phys.* **1986**, *84*, 4524.
[34] A. D. Becke, *Phys. Rev. A* **1988**, *38*, 3098.
[35] S. H. Vosko, L. Wilk, M. Nusair, *Can. J. Phys.* **1980**, *58*, 1200.
[36] J. P. Perdew, *Phys. Rev. B* **1986**, *33*, 8822.
[37] J. P. Perdew, *Phys. Rev. B* **1986**, *34*, 7406.
[38] A. Klamt, G. Schüürmann, *J. Chem. Soc. Perkin Trans. 2* **1993**, 799.
[39] J. Andzelm, C. Kölmel, A. Klamt, *J. Chem. Phys.* **1995**, *103*, 9312.
[40] A. Klamt, *J. Chem. Phys.* **1995**, *102–103*, 2224.
[41] Model implemented in the ADF package by C. C. Pye, T. Ziegler, *Theor. Chem. Acc.* **1999**, *101*, 396.

Received: June 8, 2011
Published online: November 10, 2011

